Vietnam Journal of Science and Technology
DOI: https://doi.org/10.15625/2525-2518/19779

Controlling the particle size and pore size of mesoporous SiO_2 nanoparticles for enhanced drug loading efficiency

Pham Hoai Linh[1], Tran Thi Huong[1], Nguyen Hong Nhung[1], Nguyen Quoc Dung[2], Ta Ngoc Bach[1], Nguyen Thi Ngoc Anh[1], Nguyen Thanh Nam[3], Julia A. Fedotova[4], Nguyen Tien Dung[5,*]

[1]*Institute of Materials Science, Vietnam Academy of Science and Technology, 18 Hoang Quoc Viet street, Cau Giay district, Ha Noi, Viet Nam*
[2]*Faculty of Chemistry, Thai Nguyen University of Education, No. 20 Luong Ngoc Quyen street, Thai Nguyen city, Viet Nam*
[3]*University of Transport Technology, 54 Trieu Khuc street, Thanh Xuan, Ha Noi, Viet Nam*
[4]*Institute for Nuclear Problems, Belarusian State University, Minsk 220006, Belarus*
[5]*Faculty of Chemistry, Hanoi National University of Education, 136 Xuan Thuy street, Cau Giay district, Ha Noi, Viet Nam*

[*]Email: *dungnt@hnue.edu.vn*

Received: 26 December 2023; Accepted for publication: 17 September 2025

Abstract. In this work, we focus on synthesizing mesoporous SiO_2 nanoparticles (NPs) with various sizes and pore sizes for enhancing BET surface area to apply in drug delivery by a simple modified Stöber method. By adjusting the ethanol content in the solvent mixture of cetyltrimethylammonium bromide (CTAB), four samples with particle sizes in a range of 50 nm to 350 nm and with average pore size in a range of 2.72 nm to 8.29 nm were obtained. The SiO_2 NPs exhibit a mesoporous structure with an amorphous phase, and perfect spherical morphology. The N_2 adsorption-desorption analysis reveals that mesoporous SiO_2 NPs display high BET surface values, which depend strongly on the synthesis condition as well as the particle diameters and pore sizes. The BET values increase from 848 m^2/g to 1019 m^2/g when the ethanol content in the solvents decreases from 20 % to 10 %. The Doxorubicin (DOX) loading properties were investigated as well. The highest amount of loaded DOX was achieved with 98 % loading efficiency as 99 µg/mg for the SiO_2 NPs with smallest size. The results suggest that the high surface mesoporous SiO_2 has great potential in drug delivery applications.

Keywords: SiO_2 nanoparticles, surface area, particle size, pore size, drug loading.

Classification numbers: 2.4, 2.5, 2.10.

1. INTRODUCTION

In recent years, mesoporous SiO_2 nanoparticles have attracted significant interest from the material scientists due to their potential applications in many different fields, such as catalysts, adsorbents in wastewater treatment, and petroleum adsorbents for oil spill management, …

(Mehmood *et al.*, 2017; Narayan *et al.*, 2018). In particular, mesoporous SiO_2 nanoparticles have been considered a vital representative of the innovation in material science to develop nanotechnology-based delivery systems because of their unique properties such as high biocompatibility, outstanding biodegradability, good permeability, stable structure and large pore volume and surface area (Jafari *et al.*, 2019; Karimi *et al.*, 2016; Li *et al.*, 2019; Manzano & Vallet-Regí, 2018).

Currently, many methods have been used to synthesize mesoporous SiO_2 nanoparticles (Ghaferi *et al.*, 2020), such as the Stöber method, hydrothermal, etc. Among them, the Stöber method is a simple approach for synthesizing mono-spherical silica particles. The Stöber method allows mesoporous silica nanoparticles formed following the hydrolysis and condensation of silica precursor TEOS in the solution. The biggest advantage of this method is the ability to control morphology and particle size distribution by adjusting reaction factors such as temperature, precursor concentration, pH, and additive ratio (Qiao *et al.*, 2009). However, the effect of reaction factors on the synthesis process is also complex and has not always been observed for reproducibility and consistent trends. On the other hand, the Stöber method provides SiO_2 nanoparticles with small pore volume and pore size that are unsuitable for drug carrier application (Caparrós *et al.*, 2012; Chen *et al.*, 2018; Malay *et al.*, 2013; Qiao *et al.*, 2009; Vazquez *et al.*, 2017). Thus, exploring a suitable synthesis condition to obtain products with large pore volume, controllable particle size and pore size, and well-suspended stable solution is challenging for scientists. Additionally, reports on the effect of particle size and pore size on the drug-loading capacity of SiO_2 nanoparticles are scarce.

In this study, we use a simple modified Stöber method to improve the properties of SiO_2 particles, such as surface area, pore diameter, and pore volume, for biomedical applications. SiO_2 particles were synthesized in the presence of cetyltrimethylammonium bromide (CTAB) from tetraethyl orthosilicate (TEOS) precursor and triethanolamine (TEA) catalyst in an ethanol and water medium. TEA was used as a chelating and coating agent to limit the growth and aggregation of nanoparticles (Qiao *et al.*, 2009), and the ethanol was used to guide condensation processes. By changing ethanol content in the solvent mixture of CTAB, the average particle size and the porosity of SiO_2 nanoparticles varied from 60 to 350 nm with a specific surface area higher than 1000 m^2/g. The effect of particle size and pore size on the drug loading capacity of the samples were investigated.

2. MATERIALS AND METHODS

2.1. Materials

Tetraethoxysilane ($Si(OC_2H_5)_4$) 98 %, cetyltrimethylammonium bromide ($C_{19}H_{42}BrN$) 98 %, ethanol 99.7 %, triethanolamine ($(HOCH_2CH_2)_3N$) and Doxorubicin Hydrochloride 98 %–103 % (DOX - $C_{27}H_{29}NO_{11}\cdot$ HCl) and Phosphate-buffered saline solution (PBS - 10 × concentrate) were purchased from Sigma-Aldrich. Deionized water was used in all the preparations.

2.2. Methods

SiO_2 nanoparticles were synthesized by the modified Stöber method. Typically, 2.0 g of CTAB was dissolved in 150 ml of deionized water, and a fixed amount of TEA was added to the solution to obtain pH = 10. The mixture was stirred until completely dissolved. Next,

ethanol with different volumes was added to the mixture. Then 10 mL of TEOS precursor was drop-wised to the above mixture at 60 °C and stirred for 2 hours. At the end of the reaction, the white precipitate was filtered and washed with water and ethanol to pH = 7. The white precipitate was dried at 80 °C. Finally, the SiO_2 product was obtained after heat treatment at 550 °C for 2 hours. The ethanol content in the solvent mixture of CTAB was adjusted by changing the volume ratio to 10 % (15 ml/150 ml), 13.3 % (20 ml/150 ml), 16.7 % (20 ml/150 ml), and 20 % (30 ml/150 ml) corresponding to the synthesized samples named S-E15, S-E20, S-E25, and S-E30, corresponding to the volume of ethanol in the mixture of CTAB.

2.3. Characterizations

The structure, particle size, and morphology of the synthesized samples were studied by X-ray diffraction (XRD) recorded on a D8 Advance diffractometer (Bruker) and Scanning electron microscopy (SEM) using an S-4800 microscope (Hitachi, Japan). The specific surface area of the materials was measured by BET Micromeritics 201-A. The chemical structure and chemical structures of the as-prepared samples were detected by FTIR spectroscopy (Nexus 670 FTIR).

2.4. Drug loading

Typically, 20 mg of SiO_2 nanoparticles were dispersed in the 10 ml of a DOX solution in Phosphate-buffered saline solution (PBS) with the concentration of 200 ppm under the help of a magnetic stirring in the dark. After 24 hours, 4 ml dispersed solution was withdrawn. The DOX loaded - SiO_2 nanoparticles were collected by centrifuging. The remaining DOX in the solution was determined by the intensity of UV-vis spectra at 485 nm. The drug Loading Efficiency was calculated as follows:

Drug Loading Efficiency (DLE):

$$DLE = \frac{C_t}{C_0} \times 100 \quad (1)$$

in which, C_o is the initial concentration of DOX: C_o = 200 ppm, C_t is the concentration of DOX in the SiO_2 nanoparticles: $C_t = C_0 - C_R$, C_R is the remaining concentration of DOX in the solution after adsorption process.

Drug Loading Capacity (DLC):

$$DLC = \frac{m_D}{m_0} \times 100 \quad (2)$$

m_D is the mass of DOX loading in the SiO_2 nanoparticles: $m_D = M_o - M_R$, M_0 is the initial mass of DOX, M_R is the remaining mass of DOX after adsorption process. The concentration of DOX was estimated by measuring the UV-vis absorbance at wavelength of 485 nm through the calibration curve of the relationship between the UV-vis intensity and DOX concentration (0.05, 0.1, 0.5, 1, 2.5, 5, 7.5, 10, 15, 31, 62, 125 ppm) as shown in Figure 1.

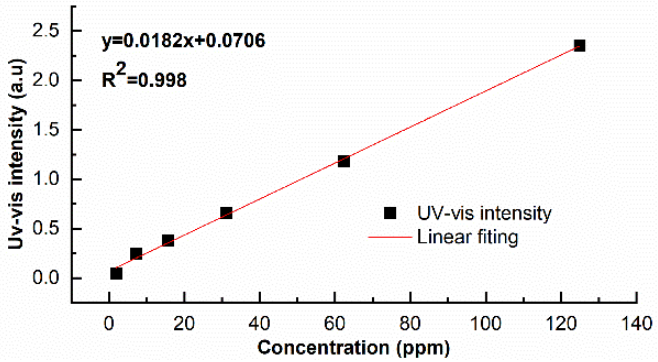

Figure 1. The calibration curve of relationship between the UV-vis intensity and DOX concentration.

3. RESULTS AND DISCUSSION

3.1. Morphology and particle size

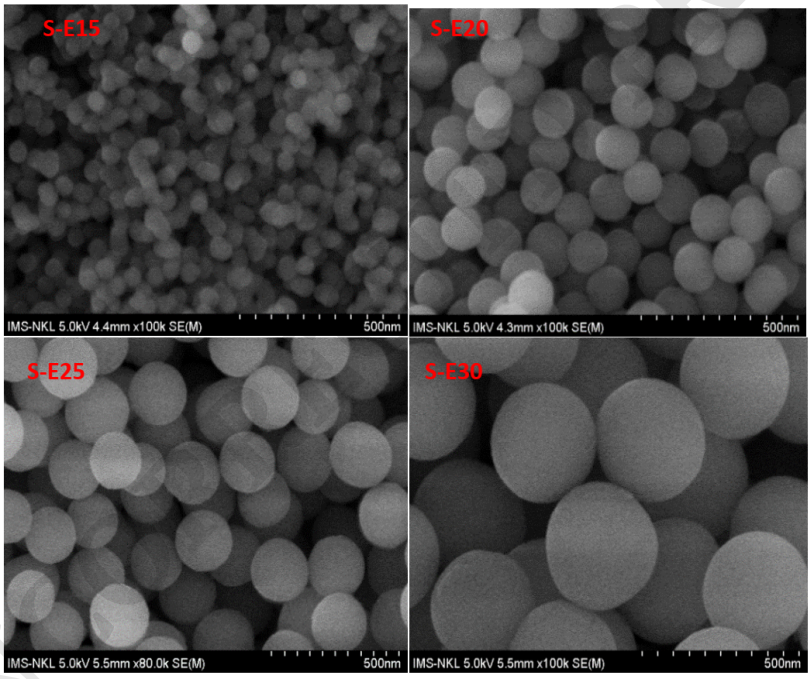

Figure 2. FE-SEM images of SiO_2 nanoparticles synthesized at different ethanol content.

Figure 2 shows the FE-SEM images of samples S-E15, S-E20, S-E25, and S-E30. It can be seen that all samples exhibit a uniform spherical in shape and clearly monodispersing. The particle sizes estimated for S-E15, S-E20, S-E25, and S-E30 samples were 52 nm, 120 nm, 185 nm, and 310 nm, respectively. According to the previous reports, SiO_2 nanoparticles in this size range have good physicochemical properties or affinity, making them suitable as carriers for efficient drug delivery (Jafari *et al.*, 2019; Manzano & Vallet-Regí, 2018). From FE-SEM images of all samples, it can be found that the particle size of mesoporous SiO_2 samples increases with the increase of ethanol content. At a low ethanol volume ratio of 15 ml, SiO_2

nanoparticles have the smallest size of 52 nm. Continuously, increasing ethanol volume ratio to 30 ml, SiO_2 nanoparticles possess particle size of 310 nm. This result could be explained by the effect of the relative water concentration in the reaction mixture on the hydrolysis and condensation processes to form nanoparticles. According to the previous reports (Chen *et al.*, 2018; Malay *et al.*, 2013), the formation of SiO_2 nanoparticles was based on the competition of the hydrolysis and condensation processes which took place through the following reactions:

Hydrolysis:

$$Si(OR)_4 + H_2O \rightleftharpoons HO\text{-}Si(OR)_3 + ROH \quad (1)$$

Alcohol condensation:

$$(OR)_3Si\text{-}OR + HO\text{-}Si(OR)_3 \rightleftharpoons (OR)_3Si\text{-}O\text{-}Si(OR)_3 + ROH \quad (2)$$

Water condensation:

$$(OR)_3Si\text{-}OH + HO\text{-}Si(OR)_3 \rightleftharpoons (OR)_3Si\text{-}O\text{-}Si(OR)_3 + H_2O \quad (3)$$

where R = alkyl group.

Accordingly, the high concentration of reactants in water accelerated the hydrolysis reaction rate (1) and reduced the rate of the condensation reaction (3). As a result, the silica particle size obtained is small. In contrast, low reactant concentration in water inhibited hydrolysis (1) and promoted condensation reactions (reactions (2) and (3)) that increased particle size. The presence of ethanol might have promoted the esterification reaction, which was the reverse hydrolysis reaction. Increasing the ethanol content in the solvent led to a decrease in the hydrolysis reaction rate while the condensation rate increased, which helped form large particles (Malay *et al.*, 2013; Vazquez *et al.*, 2017). Additionally, SiO_2 synthesis with the presence of CTAB is related to the formation of micelles resulting in a porous structure. When increasing ethanol content in the mixture of CTAB solution, the stronger interaction between CTAB tail group and ethanol leads to decreasing the size of micelles, resulting in lower pore size of mesoporous structures (Chen *et al.*, 2018). The formation process of SiO_2 nanoparticles is illustrated in Figure 3.

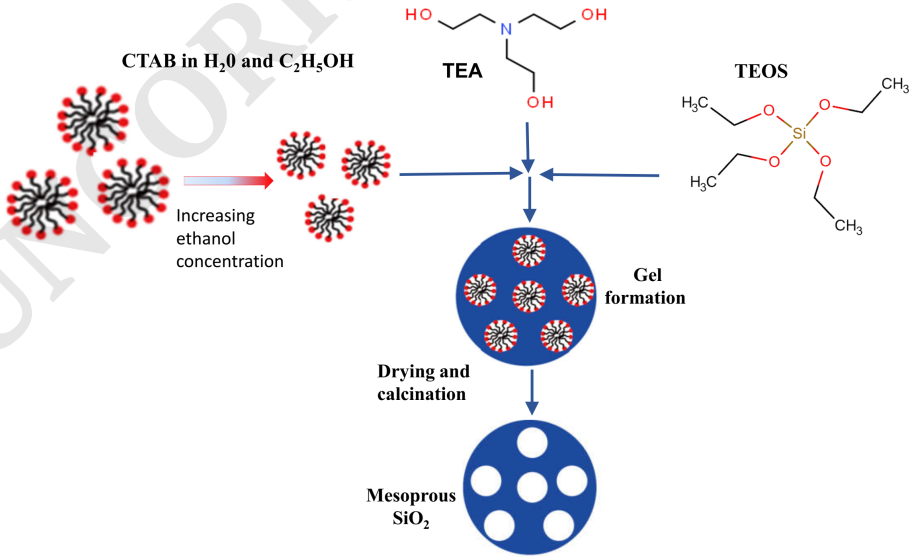

Figure 3. Schematic illustration of the formation of mesoporous SiO_2 nanoparticles.

3.2. Structure and phase

The crystalline structure of the synthesized samples was investigated by X-ray diffraction patterns as shown in Figure 4. From Figure 4, it can be observed that all samples have a broad peak centered at 23.3° that matches in good agreement with the characteristic peaks of SiO_2 nanoparticles (Caparrós *et al.*, 2012). No other impurity peak was found in the XRD diffraction patterns for all samples. The boarded peak and weak intensity reveal the amorphous material. The diffraction peaks of all samples are almost the same and not much changed. This result demonstrates that the SiO_2 particles have a similar nanostructure.

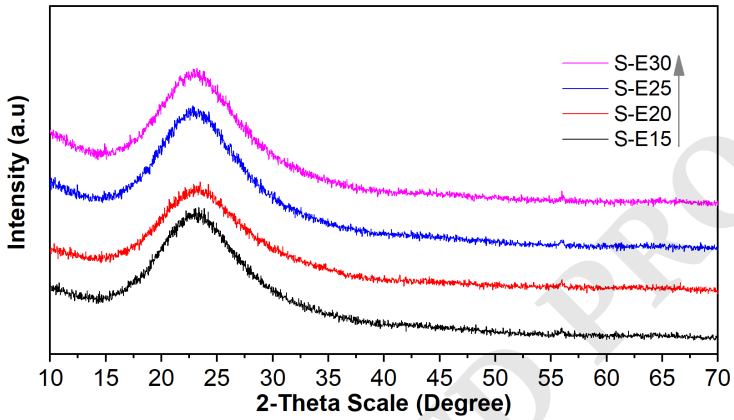

Figure 4. XRD patterns of the SiO_2 nanoparticles.

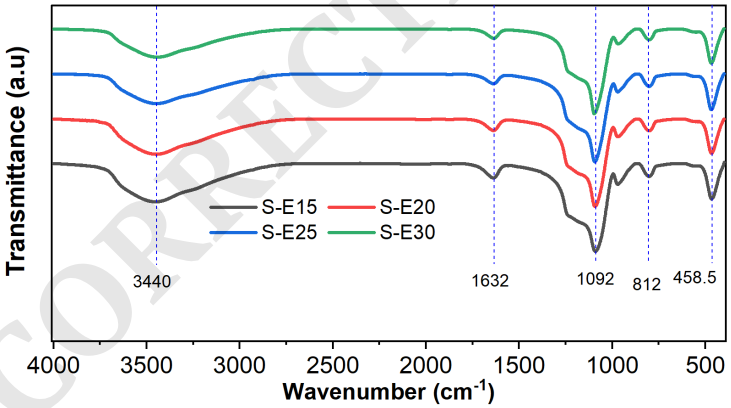

Figure 5. FTIR spectra of the synthesized SiO_2 samples.

Chemical structure of all samples were further characterized by FTIR spectra as shown in Figure 5. The broad peak from 3000 to 3700 cm^{-1} was assigned to the presence of O-H group. Similarly, a peak corresponding to vibration bending can be noticed at 1649 cm^{-1}, which indicates the presence of O-H stretching bond. The peaks at 1093 cm^{-1} and 802 cm^{-1} are attributed to the antisymmetric stretching vibration and the symmetric stretching vibration of Si-O-Si, respectively. The peak at 462 cm^{-1} is assigned to the flexural vibration of Si-O-Si, which verifies the presence of the silica structure (Xu *et al.*, 2022). From Figure 4 it can be seen that all characteristic peaks of SiO_2 almost no change when particle size increases. This reveals that the chemical structure of SiO_2 nanoparticles is unaffected by resizing.

3.3. Surface and porous properties

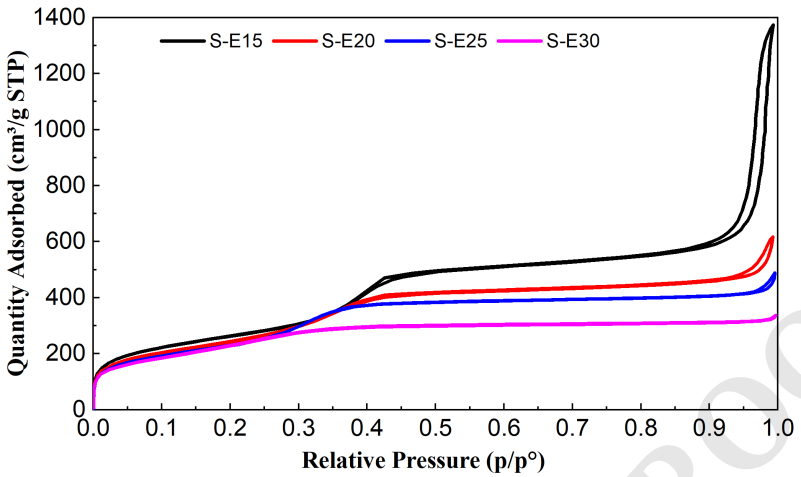

Figure. 6. The adsorption-desorption isotherm curves of nanosilica samples.

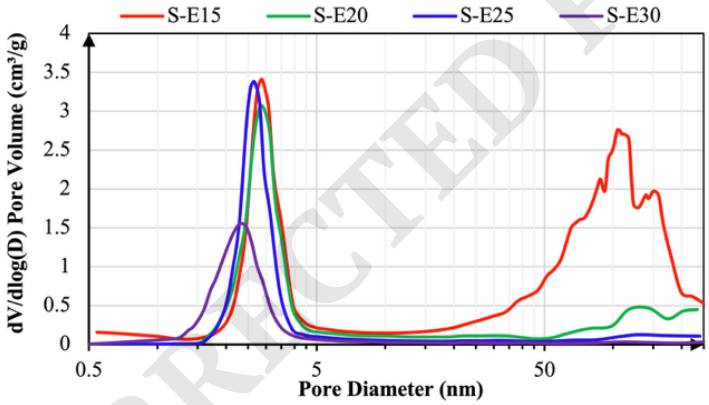

Figure 7. Diagram of pore size distribution of SiO_2 nanoparticles.

To better understand the BET surface area and porous nature of SiO_2 samples with different particle sizes, the adsorption-desorption isotherms in N_2 were carried out. The result is shown in Figure 6. All samples show type IV isothermal adsorption curves belonging to mesoporous materials. Furthermore, hysteresis loops appear for the samples S-E15, S-E20, and S-E25, which is typical for the ordered average capillary material (Ghaferi *et al.*, 2020; Qiao *et al.*, 2009). SiO_2 samples display large specific surface areas, with the calculated values listed in Table 1. From Table 1, it can be seen that surface area depends strongly on the particle size. BET values decrease with the increase of grain size originated to increasing ethanol content. Accordingly, the specific surface area according to BET is arranged in the following order: S-E15 (1019.4 m^2/g) > S-E20 (1008.4 m^2/g) > S-E25 (876.6 m^2/g) > S-E30 (848.0 m^2/g) corresponding to the increase of silica particle size (from SEM images) as follows: E15 (50–60 nm) < S-E20 (120–140 nm) < S-E25 (180–200 nm) < S-E30 (340–350 nm). Thus, the higher the ethanol content, the larger the particle size and the smaller the specific surface area. The Barrett-Joyner-Halenda (BJH) pore size distributions (Figure 7) indicate that all samples possess a mesoporous morphology. The pore volume of SiO_2 samples reached high values from 0.533 to

2.250 cm^3/g with decreasing ethanol content in the following order: S-E15 (2.250 cm^3/g) > S-E20 (1.053 cm^3/g) > S-E25 (0.852 cm^3/g) > S-E30 (0.533 cm^3/g). The BET and pore volume for SiO_2 nanoparticles obtained in our study are higher values than those described in previous reports (Caparrós *et al.*, 2012; Chen *et al.*, 2018; Ghaferi *et al.*, 2020; Karimi *et al.*, 2016). As revealed in some previous publications, the average pore diameter of nanosilica samples also tended to decrease with increasing ethanol content. These could be caused by the adhesion phenomenon of silica nanoparticles, shown in SEM images (Figure 2), forming large-sized voids and slits. Consequently, the pore diameter of sample S-E30 had the smallest average pore size of 2.72 nm. In comparison, the samples synthesized with ethanol volume below 25 ml had pore sizes that were larger than 3.5 nm, suitable for drug carriers (Karimi *et al.*, 2016; Manzano & Vallet-Regí, 2018). Especially, E-15 sample offers a larger pore size distribution of 0.8–5.2 nm. This result could be caused by the adhesion phenomenon of silica nanoparticles (as confirmed by SEM images), forming large-sized voids and slits.

Our study again confirms the role of ethanol content in the synthesis of SiO_2 by the Stöber method. Adjusting the ethanol volume ratio in the solvent mixture of CTAB could simply control the particle size and pore size of SiO_2 nanoparticles. Increasing ethanol content in the solvent mixture enhanced interaction between the CTAB tail group and ethanol. This result in reducing the size of micelles formed in the mesoporous structure. Increasing volumes of ethanol led to the smaller pore size found in the growing silica network encasing the CTAB micelles (Chen *et al.*, 2018).

Table 1. BET value, pore volume, pore size and drug loading capacity of all the SiO_2 samples.

No	Name	BET(m^2/g)	Pore volume (cm^3/g)	Pore size (nm)	DLE (%)	DLC (%)
1	S-E15	1019.4	2.250	8.29	98.5	8.9
2	S-E20	1008.4	1.053	4.22	94.2	8.6
3	S-E25	876.6	0.852	3.55	82.3	7.5
4	S-E30	848.0	0.533	2.72	86.9	7.9

To investigate the effect of particles size on the drug loading ability of SiO_2 nanoparticles, Doxorubicin hydrochloride (DOX), an anticancer drug, was used as a model drug to be loading into SiO_2 nanoparticles. Figure 8 presented the UV-vis spectra of the free DOX in the solution for all samples. The DLE and DLC values were estimated for S-E15, S-E20, S-E25, S-E30 and listed in Table 1. The obtained results show that all SiO_2 NPs exhibit the excellent DOX loading property with DLE > 82 % and DLC >= 7.5 % for all samples. The highest amount of loaded DOX was achieved with 98 % loading efficiency as 99 μg/mg. To confirm the DOX successfully loaded onto the SiO_2 samples, the FTIR spectra of S-E25 sample before and after drug loading experiment was studied and shown in Figure 9. Comparing the FTIR spectra of SiO_2 samples before and after loading DOX experiment, it can be seen that both samples exhibit the bands corresponding to the characteristics vibration modes of SiO_2 nanoparticles as mentioned in the Figure 5. From Figure 9, it can be seen that characteristic vibration mode of the pure DOX is consistent with the previous reports with the peak around at 2930 cm^{-1}, 1730 cm^{-1}, 1620 cm^{-1}, 1410 cm^{-1}, 1280 cm^{-1} and 1070 cm^{-1} correspond to the stretching vibration of the C-H bonds, C-O bonds, N-H bonds, C-C bonds, C-O-C bonds and C-O bonds, respectively (Andrade *et al.*, 2021; Kayal & Ramanujan, 2010). The observation on the FTIR spectra of the S-E25 sample after drug loading experiment reveals that the existence of the characteristic bands of DOX with peak at 2932 cm^{-1} correspond to the vibration band of C-H

bonds, the peak at 1620 cm^{-1} and 1456 cm^{-1} could be assigned to the vibration band of N-H bonds and C-C bonds. It can be also observed that in the FTIR spectrum of the S-E25 sample after drug loading, the bands characteristic of DOX at wavenumber below 1500 cm^{-1} were overlapped by the bands of the silanol and siloxane groups of SiO_2 (Andrade *et al.*, 2021). The appearance of the characteristic bands of DOX in the sample after the drug loading experiment confirms the successful loading of DOX onto the SiO_2 NP.

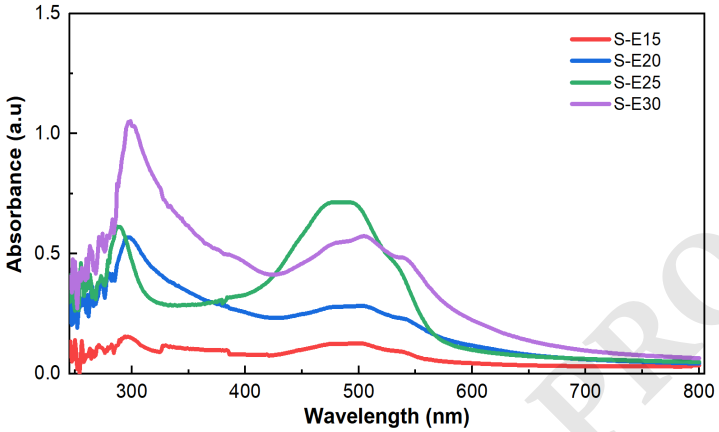

Figure 8. The UV-vis spectra of the free DOX in the solution after the drug loading experiment for the SiO_2 samples.

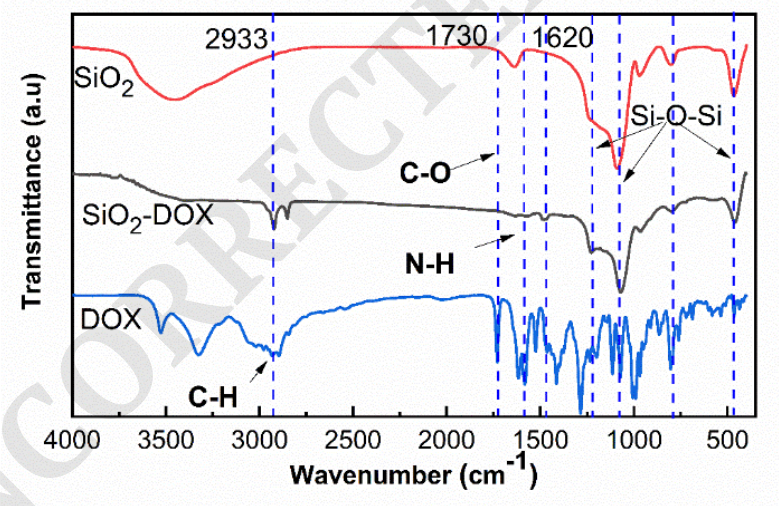

Figure 9. FTIR spectra of pure DOX and the S-E25 sample before and after drug loading experiment.

4. CONCLUSIONS

Mesoporous SiO_2 nanoparticles with different particle sizes and pore sizes have been successfully synthesized by a simple modified Stöber method. All samples exhibit spherical shapes with uniform size and porous structure in the amorphous phase. The particle size, specific surface area, pore-volume, and pore diameter of SiO_2 nanoparticles were well controlled by adjusting the ethanol content in the solvent mixture of CTAB. The specific surface area of the samples shows a large value, with the highest BET results reaching 1019 m^2/g, and

the pore volume reaching over 2.25 cm^3/g for the sample with a particle size of 52 nm. The samples show a large pore size with a wide distribution in the range of 1.8–5.1 nm. As a consequence, SiO_2 NPs possess high drug loading efficiency, with the highest value achieved at 98% loading efficiency as 99 μg/mg for the SiO_2 NPs with the smallest particle size and highest BET value. The synthesized SiO_2 nanoparticles offer great potential for application in drug delivery systems.

Acknowledgments. This work was supported by funding from the Vietnamese Ministry of Science and Technology (MOST) under Project NĐT/BY/22/16 and Vietnam Academy of Science and Technology with a Grant number QTBY01.05/21-22.

CRediT authorship contribution statement. Pham Hoai Linh: Conceptualization, Supervision, Funding acquisition. Resources, Writing - Original Draft.; Tran Thi Huong: Data curation, Methodology, Investigation, Nguyen Quoc Dung: Formal analysis. Ta Ngoc Bach: Formal analysis, Nguyen Hong Nhung: Formal analysis. Casen Panaitescu, Nguyen Thi Ngoc Anh and Nguyen Thanh Nam Conceptualization, Formal analysis, Julia A Fedotova: Funding acquisition, Methodology. Nguyen Tien Dung: Conceptualization, Writing.

Declaration of competing interest. The authors declare that they have no known competing financial interests or personal relationships that could have appeared to influence the work reported in this paper.

REFERENCES

Andrade, J. d. L., Moreira, C. A., Oliveira, A. G., de Freitas, C. F., Montanha, M. C., Hechenleitner, A. A. W., Pineda, E. A. G., & de Oliveira, D. M. F. (2021). Rice husk-derived mesoporous silica as a promising platform for chemotherapeutic drug delivery. *Waste and Biomass Valorization*, *13*(1), 241-254. https://doi.org/10.1007/s12649-021-01520-z

Caparrós, C., Benelmekki, M., Martins, P. M., Xuriguera, E., Silva, C. J. R., Martinez, L. M., & Lanceros-Méndez, S. (2012). Hydrothermal assisted synthesis of iron oxide-based magnetic silica spheres and their performance in magnetophoretic water purification. *Materials Chemistry and Physics*, *135*(2–3), 510-517. https://doi.org/10.1016/j.matchemphys.2012.05.016

Chen, Q., Ge, Y., Granbohm, H., & Hannula, S.-P. (2018). Effect of ethanol on Ag@Mesoporous silica formation by in situ modified Stöber method. *Nanomaterials*, *8*(6), 362. https://doi.org/10.3390/nano8060362

Ghaferi, M., Koohi Moftakhari Esfahani, M., Raza, A., Al Harthi, S., Ebrahimi Shahmabadi, H., & Alavi, S. E. (2020). Mesoporous silica nanoparticles: synthesis methods and their therapeutic use-recent advances. *Journal of Drug Targeting*, *29*(2), 131-154. https://doi.org/10.1080/1061186x.2020.1812614

Jafari, S., Derakhshankhah, H., Alaei, L., Fattahi, A., Varnamkhasti, B. S., & Saboury, A. A. (2019). Mesoporous silica nanoparticles for therapeutic/diagnostic applications. *Biomedicine & Pharmacotherapy*, *109*, 1100-1111. https://doi.org/10.1016/j.biopha.2018.10.167

Karimi, M., Mirshekari, H., Aliakbari, M., Sahandi-Zangabad, P., & Hamblin, M. R. (2016). Smart mesoporous silica nanoparticles for controlled-release drug delivery. *Nanotechnology Reviews*, *5*(2), 195-207. https://doi.org/10.1515/ntrev-2015-0057

Kayal, S., & Ramanujan, R. V. (2010). Doxorubicin loaded PVA coated iron oxide nanoparticles for targeted drug delivery. *Materials Science and Engineering: C*, *30*(3), 484-490. https://doi.org/10.1016/j.msec.2010.01.006

Li, Z., Zhang, Y., & Feng, N. (2019). Mesoporous silica nanoparticles: synthesis, classification, drug loading, pharmacokinetics, biocompatibility, and application in drug delivery. *Expert Opinion on Drug Delivery*, *16*(3), 219-237. https://doi.org/10.1080/17425247.2019.1575806

Malay, O., Yilgor, I., & Menceloglu, Y. Z. (2013). Effects of solvent on TEOS hydrolysis kinetics and silica particle size under basic conditions. *Journal of Sol-Gel Science and Technology*, *67*(2), 351-361. https://doi.org/10.1007/s10971-013-3088-4

Manzano, M., & Vallet-Regí, M. (2018). Mesoporous silica nanoparticles in nanomedicine applications. *Journal of Materials Science: Materials in Medicine*, *29*(5), 65. https://doi.org/10.1007/s10856-018-6069-x

Mehmood, A., Ghafar, H., Yaqoob, S., Gohar, U. F., & Ahmad, B. (2017). Mesoporous silica nanoparticles: a review. *Journal of Developing Drugs*, *06*(02), 174. https://doi.org/10.4172/2329-6631.1000174

Narayan, R., Nayak, U. Y., Raichur, A. M., & Garg, S. (2018). Mesoporous silica nanoparticles: a comprehensive review on synthesis and recent advances. *Pharmaceutics*, *10*(3), 118. https://doi.org/10.3390/pharmaceutics10030118

Qiao, Z.-A., Zhang, L., Guo, M., Liu, Y., & Huo, Q. (2009). Synthesis of mesoporous silica nanoparticles via controlled hydrolysis and condensation of silicon alkoxide. *Chemistry of Materials*, *21*(16), 3823-3829. https://doi.org/10.1021/cm901335k

Vazquez, N. I., Gonzalez, Z., Ferrari, B., & Castro, Y. (2017). Synthesis of mesoporous silica nanoparticles by sol–gel as nanocontainer for future drug delivery applications. *Boletín de la Sociedad Española de Cerámica y Vidrio*, *56*(3), 139-145. https://doi.org/10.1016/j.bsecv.2017.03.002

Xu, L., Lei, H., Ding, Z., Chen, Y., Ding, R., & Kim, T. (2022). Preparation of the rod-shaped SiO_2@C abrasive and effects of its microstructure on the polishing of zirconia ceramics. *Powder Technology*, *395*, 338-347. https://doi.org/10.1016/j.powtec.2021.09.070